ELSEVIER

International Journal of Solids and Structures 41 (2004) 1677–1695

INTERNATIONAL JOURNAL OF SOLIDS and STRUCTURES

www.elsevier.com/locate/ijsolstr

Buckling of rectangular Mindlin plates subjected to partial in-plane edge loads using the radial point interpolation method

K.M. Liew [a,b,*], X.L. Chen [a]

[a] *Nanyang Centre for Supercomputing and Visualisation, Nanyang Technological University, 50 Nanyang Avenue, Singapore 639798*

[b] *School of Mechanical and Production Engineering, Nanyang Technological University, 50 Nanyang Avenue, Singapore 639798*

Received 2 January 2003; received in revised form 20 October 2003

Abstract

This paper considers the elastic buckling of rectangular Mindlin plates that are subjected to partially distributed in-plane edge loadings. A numerical algorithm based on the radial point interpolation method (RPIM) is proposed for the solution of such plates. The pre-buckling stresses are first determined using the RPIM based on a two-dimensional (2-D) elastic plane stress problem. The buckling load intensity factors for rectangular plates that incorporate these pre-determined pre-buckling stresses are then computed via the RPIM based on the Mindlin plate theory. Numerical examples of the plates with various boundaries and subjected to different partially distributed in-plane edge loadings are presented. Shear-locking of the buckling load is studied. The results demonstrate the high accuracy of the proposed RPIM.

Keywords: Buckling loads; Mindlin plates; Partial in-plane edge loads; Radial basis function

1. Introduction

Thick plates are important structural elements, and are used in a wide range of engineering applications. They can be analyzed using the thin plate theory, but because the effects of transverse shear deformation are neglected, the deflections are underestimated and the natural frequencies and buckling loads are overestimated. Notable works on buckling and vibration of thick plates include those of Wang et al. (1993), Kitipornchai et al. (1993), Liew et al. (1995, 1996) and Cheung and Zhou (2002). The objective of this paper is to determine the elastic buckling loads of the rectangular Mindlin plates that are subjected to partial in-plane edge loads. This work is motivated by the fact that not many buckling results for this type of plates are found in the literature. To obtain results for this problem, we employed a meshless method—the radial point interpolation method (RPIM) for the analysis.

* Corresponding author. Address: Nanyang Centre for Supercomputing and Visualisation, Nanyang Technological University, 50 Nanyang Avenue, Singapore 639798. Tel.: +65-6790-4076; fax: +65-6793-6763.

E-mail address: mkmliew@ntu.edu.sg (K.M. Liew).

0020-7683/$ - see front matter © 2003 Elsevier Ltd. All rights reserved.
doi:10.1016/j.ijsolstr.2003.10.022

Existing meshless methods have their displacement interpolated according to a set of scattered nodes in the influence domain of the interpolation point. One can easily adjust the number of nodes and nodal distribution for desired computational accuracy without complex procedures. The moving least squares (MLS) technique was developed by mathematicians for data fitting and surface construction. The continuity of the MLS approximation depends mainly on the continuity of the chosen weight function. The MLS technique uses a low-order polynomial basis to construct high-order continuous approximation by choosing the appropriate weight function. Nayroles et al. (1992) were the first to employ the MLS technique to construct shape functions for their diffuse element method (DEM). Liew et al. (2002a) developed a meshless method that combined the MLS technique with the differential quadrature (DQ) method, called the MLSDQ method. Based on the DEM, Belytschko et al. (1994) proposed a different approach, called the EFG method. The EFG method uses the MLS technique to approximate displacements and the Galerkin procedure to establish weak forms of system equations. The method provides stable and highly accurate results. Liu et al. (1995) developed the reproducing kernel particle method (RKPM) by adding a correction function to the kernel to improve the smooth particle hydrodynamics (SPH) approximation near the boundaries. The modified interpolation in the RKPM satisfies consistency requirements. The shape function is smoother so that higher accuracy can be achieved for large deformation problems. Liew et al. employed the RKPM for the analysis of large deformation (2002b), free vibration of rotating cylindrical shells (2002c) and elasto-plasticity (2002d). The EFG and RKPM approximation functions are not equal to unity at nodes, and the shape functions do not have delta function properties. This complicates the imposition of essential boundary conditions.

Radial basis functions are insensitive to spatial dimension, do not depend on the direction of node to interpolation point, and are continuously differentiable and integrable. A number of radial basis functions have been used by mathematicians. Four forms of the functions with shape parameters are generally used, i.e.,

(1) multi-quadrics (MQ): $R_i(\mathbf{x}) = (r_i^2 + c^2)^q$;
(2) Gaussian (EXP): $R_i(\mathbf{x}) = \exp(-cr_i^2)$;
(3) thin plate spline (TPS): $R_i(\mathbf{x}) = r_i^\eta$;
(4) logarithmic RBF: $R_i(r_i) = r_i^\eta \log r_i$.

where r_i is the distance between the interpolation point $\mathbf{x}$ and node $\mathbf{x}_i$, c and η are the dimensionless shape parameters, and q is the constant.

The MQ radial basis function was first proposed by Hardy (1990) for the interpolation of geographical scattered data. The MQ radial basis function has been widely used in surface fitting and in constructing approximate solution for partial differential equations (Kansa, 1990). The MQ radial basis function was used in the PIM by Wang and Liu (2002).

The treatment of buckling of plates that are subjected to partially distributed in-plane edge loadings with non-uniform pre-buckling stresses is generally more involved. First we must deal with the pre-buckling stresses that are non-uniform near the in-plane edge loadings. The complex nature of the pre-buckling stress field makes it almost impossible to obtain an exact solution for this problem. Hence, the RPIM is implemented in the buckling analysis of Mindlin plates that are subjected to partially distributed in-plane edge loadings. The pre-buckling stresses of the plates are first determined using the RPIM based on a two-dimensional (2-D) elastic plane stress problem. The buckling loads of the plates with these predetermined pre-buckling stresses are then computed by the RPIM based on the Mindlin plate theory. The *ANSYS* software package, a type of finite element (FE) software, is also employed to calculate the buckling loads of the plates for comparison. Numerical examples of Mindlin plates with different boundary conditions and subjected to partially distributed in-plane edge loadings are presented. This study shows that the RPIM is able to produce results with high accuracy.

2. Displacement interpolation based on RPIM

A displacement $u(\mathbf{x})$ ($\mathbf{x} \in \{x, y\}$) in the problem domain is interpolated in a small neighborhood of interpolation point $\mathbf{x}$ by using a radial basis function and polynomial basis (Wang and Liu, 2002) in the RPIM, and is defined by

$$u(\mathbf{x}) = \sum_{i=1}^{n} R_i(\mathbf{x}) a_i + \sum_{j=1}^{m} P_j(\mathbf{x}) b_j \tag{1}$$

where $R_i(\mathbf{x})$ is the radial basis function, a_i is the unknown coefficient that corresponds to the radial basis function, n is the number of nodes in the influence domain of interpolation point $\mathbf{x}$, $P_j(\mathbf{x})$ is the polynomial basis that has m polynomial terms, and b_j is the unknown coefficient corresponding to the polynomial basis. The interpolation function passes through all of the nodes in the influence domain. For one-dimensional problems, the schematic interpolation function $u^h(x)$ is drawn in Fig. 1. The approximated value $u^h(x_i)$ of node x_i is equal to the nodal displacement u_i.

The multi-quadrics (MQ) radial basis function is chosen, i.e.,

$$R_i(\mathbf{x}) = [r_i^2 + (\alpha_q \Delta r)^2]^q \tag{2}$$

where α_q is the dimensionless shape parameter, q is the constant, r_i is the space distance between node $\mathbf{x}_i$ and interpolation point $\mathbf{x}$, and Δr is the average nodal space distance.

The polynomial basis $P_j(\mathbf{x})$ is chosen according to Pascal's triangle. Generally, it is chosen as a complete polynomial basis for computational accuracy. The number of nodes n in the influence domain of point $\mathbf{x}$ is chosen to be larger than the terms m of polynomial basis ($n > m$), based on the reproduction requirement.

In the RPIM, displacement interpolation of any interpolation point $\mathbf{x}$ must pass through all of the n nodes in the influence domain of point $\mathbf{x}$. The interpolated displacement can be expressed as

$$u^{\mathrm{l}}(\mathbf{x}_k) = \sum_{i=1}^{n} R_i^{\mathrm{l}}(\mathbf{x}_k) a_i^{\mathrm{l}} + \sum_{j=1}^{m} P_j^{\mathrm{l}}(\mathbf{x}_k) b_j^{\mathrm{l}} \quad \text{for } k = 1, 2, \ldots, n \tag{3}$$

where the superscript l means that the variables in Eq. (3) are local variables in the small influence domain of the interpolation point $\mathbf{x}$.

The polynomial basis needs to satisfy an extra requirement to guarantee unique approximation (Golberg et al., 1999), and the extra requirement is usually taken as the following constraint forms:

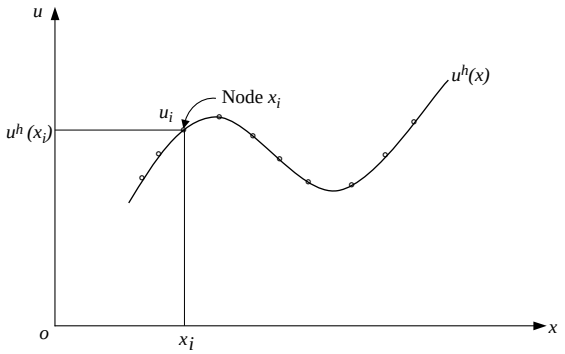

Fig. 1. A schematic interpolation function $u^h(x)$, approximated value $u^h(x_i)$ and nodal displacement u_i of node x_i in the RPIM technique.

$$\sum_{i=1}^{n} P_j^1(\mathbf{x}_i)a_i^1 = 0 \quad \text{for } j = 1, 2, \ldots, m \tag{4}$$

The unknown coefficients a_i and b_j can be solved through the combination of Eqs. (3) and (4). Substituting these coefficients into Eq. (1) gives the displacement interpolation function in the form of

$$u(\mathbf{x}) = \sum_{i=1}^{n} \phi_i(\mathbf{x})u_i \tag{5}$$

where $\phi_i(\mathbf{x})$ is the shape function for a node $\mathbf{x}_i$. The shape functions satisfy the following conditions:

$$\phi_i(\mathbf{x}_i) = 1 \quad \text{for } i = 1, 2, \ldots, n \tag{6a}$$

$$\phi_j(\mathbf{x}_i) = 0 \quad \text{for } j \neq i \tag{6b}$$

$$\sum_{i=1}^{n} \phi_i(\mathbf{x}) = 1 \tag{6c}$$

3. Governing equations

When a plate is subjected to non-uniform in-plane edge loadings, the resultant stress distribution in the plate is non-uniform. To obtain the value of buckling loads of the plate, we must first obtain the pre-buckling stress distribution. The RPIM is developed for first solving the non-uniform pre-buckling stress distribution, and then the buckling loads. Two separate FORTRAN programs are coded based on the present RPIM. The first program is used to compute the pre-buckling stress distribution in the plate based on a 2-D elastic plane stress problem. The second program is used to determine the buckling loads of the plate with the pre-buckling stress distribution that is obtained from the first program based on the Mindlin plate assumption.

3.1. Governing equations for solving pre-buckling stress distribution

When a plate is subjected to in-plane edge loadings, it can be treated as 2-D elastic plane stress problem for computing the pre-buckling stress distribution. The variational form of the equilibrium equation of the static 2-D elastic plane stress problem is

$$\int_V \delta(\nabla_s \mathbf{u}_s)^t \cdot \boldsymbol{\sigma}\, \mathrm{d}V - \int_V \delta\mathbf{u}_s^t \cdot \mathbf{b}\, \mathrm{d}V - \int_{S_\sigma} \delta\mathbf{u}_s^t \cdot \bar{\mathbf{t}}\, \mathrm{d}S = 0 \tag{7}$$

where $\boldsymbol{\sigma}$ is the stress field, $\mathbf{u}_s$ is the displacement field, $\mathbf{b}$ is the body forces, $\bar{\mathbf{t}}$ is the surface forces, and ∇_s is the derivative operator that is defined by

$$\nabla_s = \begin{bmatrix} \partial/\partial x & 0 \\ 0 & \partial/\partial y \\ \partial/\partial y & \partial/\partial x \end{bmatrix} \tag{8}$$

The RPIM is employed to implement the displacement interpolation $\mathbf{u}_s$ based on a set of scattered nodes in a small influence domain of interpolation point $\mathbf{x}$. According to Eq. (5), the displacement field $\mathbf{u}_s$ can be interpolated as

$$\mathbf{u}_s = \begin{Bmatrix} u \\ v \end{Bmatrix} = \sum_{i=1}^{n} \begin{bmatrix} \phi_i & 0 \\ 0 & \phi_i \end{bmatrix} \begin{Bmatrix} u_i \\ v_i \end{Bmatrix} \tag{9}$$

By substituting the approximated displacements $\mathbf{u}_s$ of Eq. (9) into the variational form of Eq. (7), the discrete system equation of 2-D elastic plane stress problem becomes

$$\mathbf{K}_{ij}\mathbf{u}_j = \mathbf{f}_i \quad \text{for } i = 1, 2, \ldots, n \text{ and } j = 1, 2, \ldots, n \tag{10}$$

where $\mathbf{K}_{ij}$ is the stiffness matrix, $\mathbf{f}_i$ is the force vector, and $\mathbf{u}_j$ is the displacements of node $\mathbf{x}_j$ that is defined by

$$\mathbf{u}_j = \begin{Bmatrix} u_j \\ v_j \end{Bmatrix} \tag{11}$$

The stiffness matrix $\mathbf{K}_{ij}$ can be written as

$$\mathbf{K}_{ij} = \int_V \mathbf{B}_i^t \mathbf{D}_s \mathbf{B}_j \, \mathrm{d}V \tag{12}$$

where

$$\mathbf{B}_i = \begin{bmatrix} \partial\phi_i/\partial x & 0 \\ 0 & \partial\phi_i/\partial y \\ \partial\phi_i/\partial y & \partial\phi_i/\partial x \end{bmatrix} \tag{13}$$

$$\mathbf{D}_s = \frac{E}{1-v^2} \begin{bmatrix} 1 & v & 0 \\ v & 1 & 0 \\ 0 & 0 & (1-v)/2 \end{bmatrix} \tag{14}$$

in which E is the elastic rigidity and v is Poisson's ratio.

The force vector $\mathbf{f}_i$ can be written as

$$\mathbf{f}_i = \begin{Bmatrix} f_{xi} \\ f_{yi} \end{Bmatrix} = \int_V \begin{Bmatrix} \phi_i b_x \\ \phi_i b_y \end{Bmatrix} \mathrm{d}V + \int_{S_\sigma} \begin{Bmatrix} \phi_i \bar{t}_x \\ \phi_i \bar{t}_y \end{Bmatrix} \mathrm{d}S \tag{15}$$

The displacements of the 2-D elastic plane stress problem can be solved from Eq. (10). Thus, the pre-buckling stress field of any point can be calculated as

$$\boldsymbol{\sigma} = \begin{Bmatrix} \sigma_x^0 \\ \sigma_y^0 \\ \tau_{xy}^0 \end{Bmatrix} = \sum_{i=1}^{n} \mathbf{D}_s \mathbf{B}_i \mathbf{u}_i \tag{16}$$

3.2. Governing equations for solving buckling loads of Mindlin plate

For the static buckling analysis of a plate, the variational form of the total potential energy of the plate can be written as

$$\delta\Pi = \int_V \delta(\nabla_b \mathbf{u}_b)^t \cdot \boldsymbol{\sigma}_b \, \mathrm{d}V + \int_V \delta\boldsymbol{\varepsilon}_n^t \cdot \boldsymbol{\tau}_n \, \mathrm{d}V = 0 \tag{17}$$

where $\mathbf{u}_b$ is the displacement field of the plate, $\boldsymbol{\sigma}_b$ is the linear stress field of the plate, $\boldsymbol{\varepsilon}_n$ is the non-linear strain field of the plate, $\boldsymbol{\tau}_n$ is the pre-buckling stress field of the plate, and ∇_b is the derivative operator that is defined by

$$\nabla_b = \begin{bmatrix} \partial/\partial x & 0 & 0 \\ 0 & \partial/\partial y & 0 \\ \partial/\partial y & \partial/\partial x & 0 \\ \partial/\partial z & 0 & \partial/\partial x \\ 0 & \partial/\partial z & \partial/\partial y \end{bmatrix} \tag{18}$$

For a plate that is based on Mindlin's plate assumption (Liew et al., 1996), there are three independent displacement variables (see Fig. 2): transverse deflection w of a point on the mid-plane, rotation φ_x about the y-axis, and rotation φ_y about the x-axis. These three independent variables can be interpolated based on a set of scattered nodes in a small influence domain of interpolation point $\mathbf{x}$. According to Eq. (5), the displacement field $\mathbf{u}_b$ can be interpolated as

$$\mathbf{u}_b(x,y,z) = \begin{Bmatrix} u(x,y,z) \\ v(x,y,z) \\ w(x,y,z) \end{Bmatrix} = \begin{Bmatrix} z\varphi_x(x,y) \\ z\varphi_y(x,y) \\ w(x,y) \end{Bmatrix} = \begin{Bmatrix} z\sum_{i=1}^{n}\phi_i\varphi_{xi} \\ z\sum_{i=1}^{n}\phi_i\varphi_{yi} \\ \sum_{i=1}^{n}\phi_i w_i \end{Bmatrix} \tag{19}$$

The non-linear strain field $\boldsymbol{\varepsilon}_n$ can be expressed as

$$\boldsymbol{\varepsilon}_n = \begin{Bmatrix} \varepsilon_x^0 \\ \varepsilon_y^0 \\ \gamma_{xy}^0 \\ \gamma_{xz}^0 \\ \gamma_{yz}^0 \end{Bmatrix} = \begin{Bmatrix} \frac{1}{2}(\partial w/\partial x)^2 + \frac{1}{2}(\partial\varphi_x/\partial x)^2 + \frac{1}{2}(\partial\varphi_y/\partial x)^2 \\ \frac{1}{2}(\partial w/\partial y)^2 + \frac{1}{2}(\partial\varphi_x/\partial y)^2 + \frac{1}{2}(\partial\varphi_y/\partial y)^2 \\ (\partial w/\partial x)(\partial w/\partial y) + (\partial\varphi_x/\partial x)(\partial\varphi_x/\partial y) + (\partial\varphi_y/\partial x)(\partial\varphi_y/\partial y) \\ 0 \\ 0 \end{Bmatrix} \tag{20}$$

The higher order terms of $\boldsymbol{\varepsilon}_n$ in Eq. (20) can be omitted (Wang et al., 1993). Therefore, $\boldsymbol{\varepsilon}_n$ can be simplified as

$$\boldsymbol{\varepsilon}_n = \begin{Bmatrix} \frac{1}{2}(\partial w/\partial x)^2 \\ \frac{1}{2}(\partial w/\partial y)^2 \\ (\partial w/\partial x)(\partial w/\partial y) \\ 0 \\ 0 \end{Bmatrix} \tag{21}$$

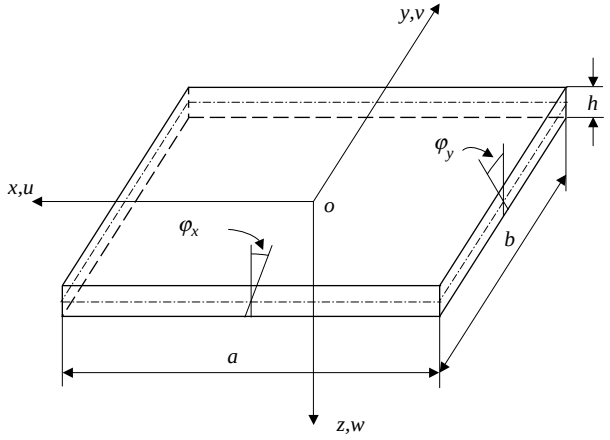

Fig. 2. Mindlin plate, its co-ordinate system, and geometrical notation.

The pre-buckling stress field $\boldsymbol{\tau}_n$ that is produced by in-plane edge loadings can be written as

$$\boldsymbol{\tau}_n = \begin{Bmatrix} \sigma_x^0 \\ \sigma_y^0 \\ \tau_{xy}^0 \\ \tau_{xz}^0 \\ \tau_{yz}^0 \end{Bmatrix} = \begin{Bmatrix} \sigma_x^0 \\ \sigma_y^0 \\ \tau_{xy}^0 \\ 0 \\ 0 \end{Bmatrix} \tag{22}$$

Substituting the approximated displacements $\mathbf{u}_b$ of Eq. (19) into the variational form of Eq. (17), the discrete eigenvalue equation of the static buckling problem of Mindlin plates can be derived as

$$[\overline{\mathbf{K}}_{ij} + P_{\mathrm{cr}}\overline{\mathbf{H}}_{ij}]\overline{\mathbf{U}}_j = 0 \quad \text{for } i = 1, 2, \ldots, n \text{ and } j = 1, 2, \ldots, n \tag{23}$$

where P_{cr} is the eigenvalues, and $\overline{\mathbf{K}}_{ij}$, $\overline{\mathbf{H}}_{ij}$, and $\overline{\mathbf{U}}_j$ are defined by

$$\overline{\mathbf{K}}_{ij} = \int_V \overline{\mathbf{B}}_i^t \mathbf{D}_b \overline{\mathbf{B}}_j \, \mathrm{d}V \tag{24}$$

$$\overline{\mathbf{H}}_{ij} = \begin{bmatrix} \overline{H}_{ij}^p & 0 & 0 \\ 0 & 0 & 0 \\ 0 & 0 & 0 \end{bmatrix} \tag{25}$$

$$\overline{\mathbf{U}}_j = \begin{Bmatrix} \varphi_{xj} \\ \varphi_{yj} \\ w_j \end{Bmatrix} \tag{26}$$

in which

$$\overline{\mathbf{B}}_i = \begin{bmatrix} 0 & z\partial\phi_i/\partial x & 0 \\ 0 & 0 & z\partial\phi_i/\partial y \\ 0 & z\partial\phi_i/\partial y & z\partial\phi_i/\partial x \\ \partial\phi_i/\partial x & \phi_i & 0 \\ \partial\phi_i/\partial y & 0 & \phi_i \end{bmatrix} \tag{27}$$

$$\mathbf{D}_b = E/(1-\nu^2)\begin{bmatrix} 1 & \nu & 0 & 0 & 0 \\ \nu & 1 & 0 & 0 & 0 \\ 0 & 0 & (1-\nu)/2 & 0 & 0 \\ 0 & 0 & 0 & k_s(1-\nu)/2 & 0 \\ 0 & 0 & 0 & 0 & k_s(1-\nu)/2 \end{bmatrix} \tag{28}$$

$$\overline{H}_{ij}^p = \int_V [\sigma_x^0(\partial\phi_i/\partial x)(\partial\phi_j/\partial x) + \sigma_y^0(\partial\phi_i/\partial y)(\partial\phi_j/\partial y) + \tau_{xy}^0\{(\partial\phi_i/\partial x)(\partial\phi_j/\partial y) + (\partial\phi_j/\partial x)(\partial\phi_i/\partial y)\}]\,\mathrm{d}V \tag{29}$$

and k_s is the shear correction factor with a value of $k_s = 5/6$ adopted for Mindlin plates.

The shape functions that are employed in the RPIM satisfy the delta function property, i.e., the approximated displacement at one node is equal to its nodal displacement, and essential boundary conditions can be directly imposed on the discrete eigenvalue equation (Eq. (23)) using the same procedure as used in the FEM. Solving Eq. (23) gives a set of eigenvalues and a corresponding set of eigenvectors. The eigenvalues give the static buckling loads, and the eigenvectors give the buckling modes of the corresponding buckling loads.

4. Example problems

The present RPIM is formulated for calculating pre-buckling stress distribution and buckling loads of square Mindlin plates with different boundaries and subjected to different in-plane edge loadings. Some parameters of the square Mindlin plates are as follows:

Edge length $a = b = 10$ (m);
Young's modulus $E = 200.0 \times 10^9$ (N/m^2);
Poisson's ratio $v = 0.3$.

Wang and Liu (2002) studied the choice of the shape parameter and the constant of the MQ radial basis function and their influence on the stress solution for beam structures. This approach offers highly accurate and stable results. Hence, we choose the shape parameter and constant of the MQ radial basis function as $\alpha_q = 2.0$ and $q = 1.03$.

Polynomial term $m = 3$ is taken (i.e., polynomial bases are $\{1, x, y\}$).

In all of the numerical examples except for special illustration, when the present RPIM is used to calculate pre-buckling stress distributions and buckling loads of the plates, the size of quadrilateral influence domain $d_{\max}$ is chosen to be 3.0 times the average nodal distance. Quadrilateral integration background cells 15×15 are regularly distributed in the entire domain of the plates. Gauss points 4×4 at each integration background cell are chosen. Nodes 16×16 are regularly distributed in the entire domain of the plates.

To compare the present RPIM results with FEM results, *ANSYS* is used to calculate buckling loads of the plates. 24×24 elements with element type *four-noded shell 63* and the *Block Lanczos* method are used.

In all tables and figures, the notations SSSS and CCCC denote simply supported and clamped at four edges of the plates, respectively. The notation CFCF denotes that the two edges which are parallel to the y-axis are clamped while the other two edges are free.

The buckling load parameter of the plates that are subjected to in-plane edge loadings is defined as $k_p = P_{\mathrm{cr}} b/D_0$, where P_{cr} is critical in-plane edge loading and $D_0 = Eh^3/12(1-v^2)$ is elastic rigidity.

4.1. Verification studies

The square Mindlin plate ($a/b = 1$) that is shown in Fig. 3 under a simply supported boundary condition is considered for studying the convergence of buckling load parameters. The thickness ratio of the plate is taken as $h/b = 0.01$. The plate is subjected to three in-plane edge loadings: uniform edge loadings ($c/b = 1$); partial uniform edge loadings ($c/b = 0.5$); and concentrated edge loadings ($c/b = 0$). Different numbers of nodes in the plate domain are used. The buckling load parameter is normalized as k_p/k_p^0, where k_p is the present buckling load parameter and k_p^0 is the buckling load parameter given by published literature or the FEM result obtained by *ANSYS*. For plates that are subjected to uniform edge loadings ($c/b = 1$), $k_p^0 = 39.478$, which is presented by Timoshenko and James (1985). For plates that are subjected to partial uniform edge loadings ($c/b = 0.5$), to the best of the authors' knowledge no results are available in existing literature. Therefore, we obtained the results by using *ANSYS* (24×24 elements with element type *four-noded shell 63*). In this case, $k_p^0 = 30.666$. For plates that are subjected to concentrated edge loadings ($c/b = 0$), the Leissa and Ayoub (1988) solution is $k_p^0 = 25.814$. The normalized buckling load parameters that we computed, using different numbers of nodes, are depicted in Fig. 4. The patch test for the interpolation function of the RPIM has been given in the literature (Wang and Liu, 2002). The RPIM cannot, in general, easily pass the patch test. It passes the patch test of the linear displacement when polynomial terms $m = 3$ (i.e., linear polynomial basis). It failed to pass the linear displacement patch when no polynomial terms are included. It can be observed from Fig. 4 that the buckling load parameters oscillate, especially for

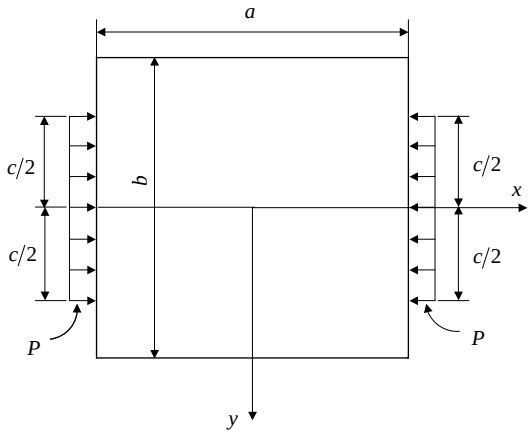

Fig. 3. A square plate that is subjected to axial in-plane edge loadings.

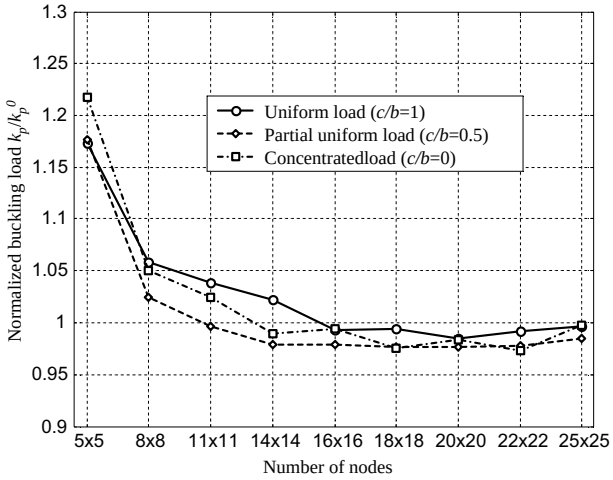

Fig. 4. Convergence study of the buckling load parameters of the simply supported square plate that is subjected to axial in-plane edge loadings.

the concentrated load case. When over 16×16 nodes are used, the normalized buckling load parameters fall in a very small range, although they oscillate. A comparison of the results is presented in the first column of Table 1, and shows the good agreement of the present results with the FEM solutions and the results that were given by Leissa and Ayoub (1988) and Timoshenko and James (1985).

4.2. Results and discussions

The first example considered is a square Mindlin plate, as shown in Fig. 3, that is subjected to uniform edge loadings ($c/b = 1$) with different thickness ratios and boundary conditions. Two thickness ratios, $h/b = 0.1$ and $h/b = 0.05$, and three essential boundary conditions, SSSS, CCCC, and CFCF, are

Table 1
Buckling load parameters $k_p = P_{cr}b/D_0$ for a square Mindlin plate that is subjected to axial in-plane edge loadings ($h/b = 0.01$)

c/b	Boundaries		
	SSSS	CCCC	CFCF
0	25.659 (25.636[a], 25.814[b])	67.712 (66.057[a])	36.290 (35.982[a])
0.25	26.925 (27.160[a])	70.925 (70.733[a])	36.887 (36.759[a])
0.5	30.024 (30.666[a])	81.024 (81.277[a])	38.656 (38.484[a])
1.0	39.183 (40.105[a], 39.478[c])	100.178 (100.561[a], 99.387[c])	38.894 (38.549[a])

[a] Results of FEM (*ANSYS*).
[b] Results of Leissa and Ayoub (1988).
[c] Results of Timoshenko and James (1985).

Table 2
Buckling load parameters $k_p = P_{cr}b/D_0$ for a square Mindlin plate that is subjected to axial in-plane uniform edge loadings

Thickness ratio, h/b	Boundaries	RPIM	Kitipornchai et al. (1993)
0.1	SSSS	37.36	37.38
	CCCC	81.85	81.84
	CFCF	34.68	34.62
0.05	SSSS	38.95	38.93
	CCCC	94.57	94.34
	CFCF	37.69	37.51

considered. The results are shown in Table 2. It is evident that the present buckling load parameters agree very well with the analytical solutions (Kitipornchai et al., 1993). The buckling load parameters of the plate increase as the plate thickness decreases. The square Mindlin plate is now considered with four kinds of

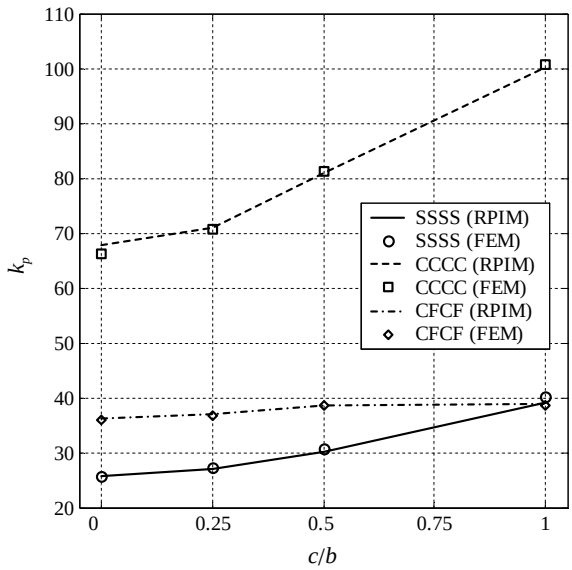

Fig. 5. The buckling load parameters of the square plate that is subjected to axial in-plane edge loadings.

axial in-plane edge loadings ($c/b = 0$, 0.25, 0.5, 1.0). The thickness ratio of the plate is taken as $h/b = 0.01$. *ANSYS* is used to calculate its buckling loads. The RPIM buckling load parameters, FEM results, and other available results are listed in Table 1. The RPIM buckling load parameters and FEM results are also drawn in Fig. 5. It is obvious that the RPIM buckling load parameters are in close agreement with the available results and FEM results.

The shear-locking of the buckling load of a simply supported thin square plate that is subjected to uniform axial in-plane edge loadings is studied. The thickness-to-width is $h/b = 0.001$. Because the desired high-order approximated displacement fields can be obtained easily in the RPIM, those for one transverse deflection and two rotations are constructed to relieve shear-locking by simply using high-order polynomial

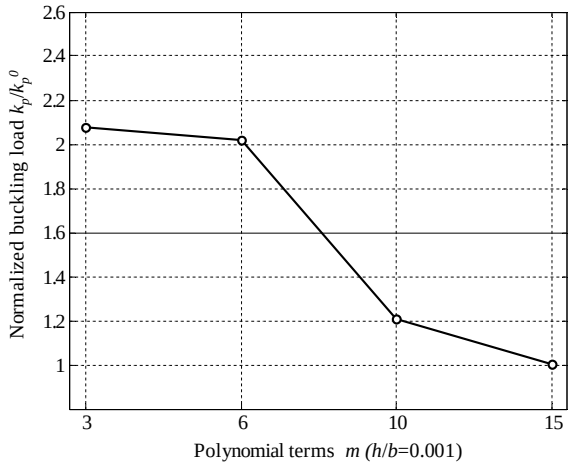

Fig. 6. Shear-locking study of the buckling load of the simply supported thin square plate that is subjected to uniform axial in-plane edge loadings.

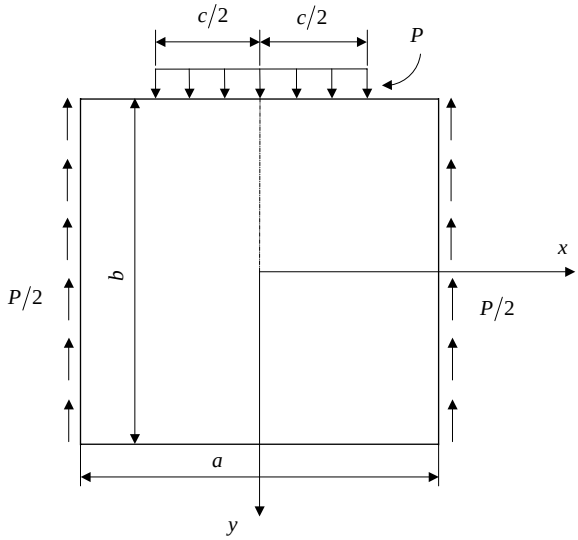

Fig. 7. A square plate that is subjected to axial and shear in-plane edge loadings.

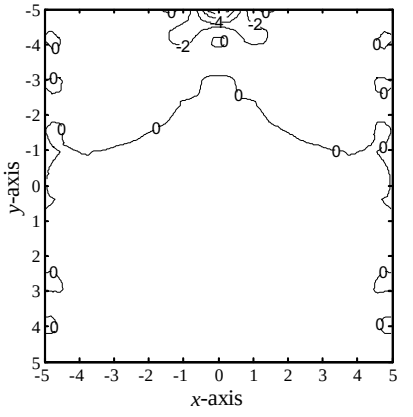

(a) $c/a = 0$

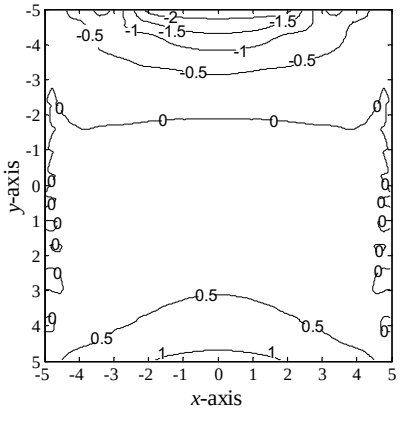

(b) $c/a = 0.5$

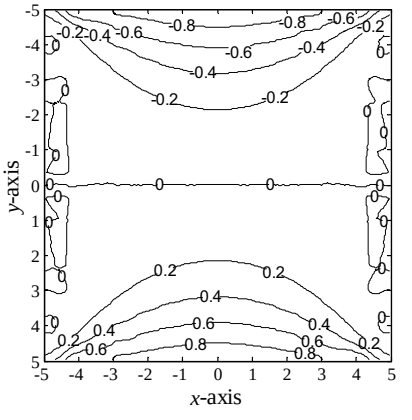

(c) $c/a = 1$

Fig. 8. (a–c) Non-dimensional stresses $\sigma_x^0 bh/P$ of the simply supported square plate that is subjected to axial and shear in-plane edge loadings.

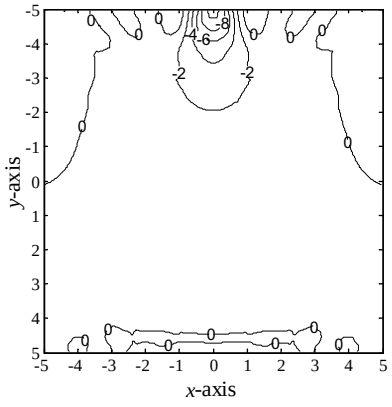

(a) $c/a = 0$

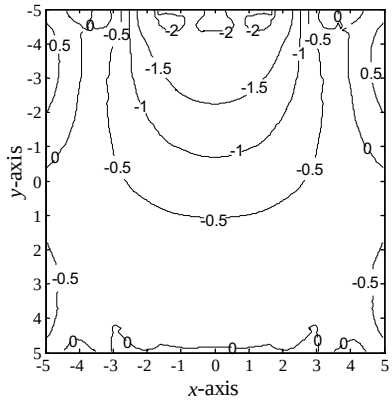

(b) $c/a = 5.0$

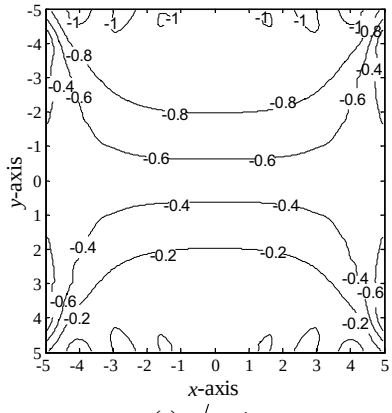

(c) $c/a = 1$

Fig. 9. (a–c) Non-dimensional stresses $\sigma_y^0 bh/P$ of the simply supported square plate that is subjected to axial and shear in-plane edge loadings.

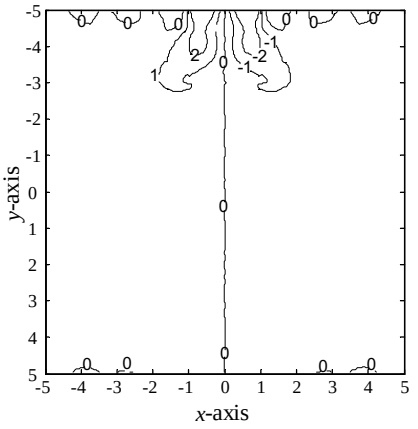

(a) $c/a = 0$

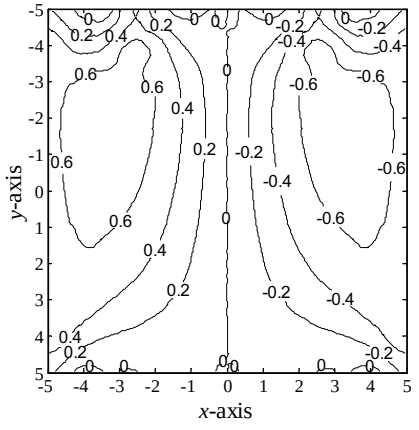

(b) $c/a = 0.5$

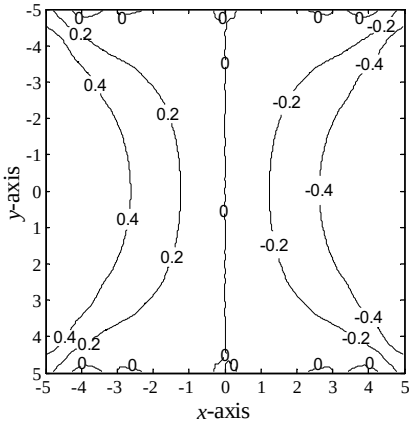

(c) $c/a = 1$

Fig. 10. (a–c) Non-dimensional stresses $\tau^0_{xy} bh/P$ of the simply supported square plate that is subjected to axial and shear in-plane edge loadings.

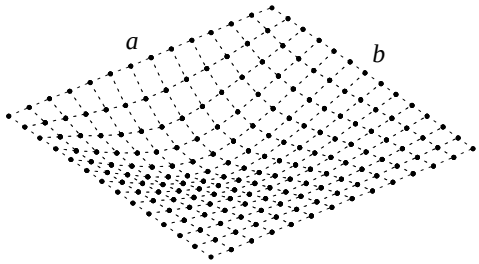

(a) $c/a = 0$

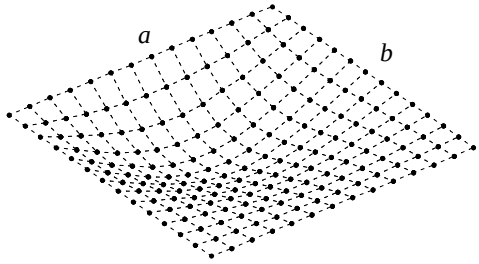

(b) $c/a = 0.5$

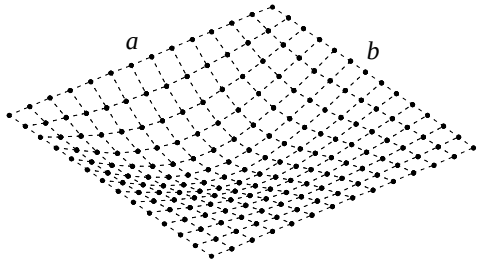

(c) $c/a = 1$

Fig. 11. (a–c) Buckling mode shapes of the simply supported square plate that is subjected to axial and shear in-plane edge loadings.

terms. The polynomial basis is chosen according to Pascal's triangle. The same number of polynomial terms is used for one transverse deflection and two rotations' approximations. 18×18 nodes in the whole plate domain are used. The size of quadrilateral influence domain $d_{\max}$ is chosen to be 3.0 times the average nodal distance for polynomial terms 3, 6, and 10. As the terms of the polynomial basis increase, more nodes must be included in the influence domain of a selected point to approximate displacements. The size of the influence domain $d_{\max}$ is chosen to be 4.5 times the average nodal distance when 15 polynomial terms are used. The normalized buckling load parameters are shown in Fig. 6. The shear-locking phenomenon is observed very clearly when only three polynomial terms are used, i.e., the normalized buckling load parameter becomes too big. The shear-locking is gradually relieved as the polynomial terms are increased. When the terms of the polynomial basis up to 15 are used, the shear-locking is eliminated.

The second example is a square Mindlin plate that is subjected to axial and shear in-plane edge loadings, as shown in Fig. 7. The two edges that are parallel to the y-axis are applied with uniform shear loads. The top edge that is parallel to the x-axis is applied with a concentrated load ($c/a = 0$), partial uniform load ($c/a = 0.25$ and 0.5), or uniform load ($c/a = 1$). The thickness ratio of the plate is taken as

Table 3
Buckling load parameters $k_p = P_{cr}b/D_0$ for a square Mindlin plate that is subjected to axial and shear in-plane edge loadings ($h/b = 0.01$)

c/a	Boundaries		
	SSSS	CCCC	CFCF
0	32.371 (32.129[a])	82.075 (80.182[a])	13.332 (13.366[a])
0.25	34.042 (34.559[a])	86.438 (86.272[a])	14.813 (14.918[a])
0.5	39.051 (39.888[a])	100.423 (100.529[a])	19.270 (19.352[a])
1.0	56.646 (56.335[a])	144.575 (143.041[a])	34.646 (34.627[a])

[a] Results of FEM (*ANSYS*).

$h/b = 0.01$. Three cases of essential boundary conditions, SSSS, CCCC, and CFCF, are considered. The pre-buckling stresses of the square Mindlin plate for the loading cases $c/a = 0, 0.5$, and 1.0 are computed using the RPIM. The non-dimensional stresses $\sigma_x^0 bh/P$, $\sigma_y^0 bh/P$, and $\tau_{xy}^0 bh/P$ of all the Gaussian points in the entire plate domain are plotted in Figs. 8–10(a)–(c), respectively. The non-dimensional normal stresses $\sigma_x^0 bh/P$ and $\sigma_y^0 bh/P$, are symmetrical about the y-axis, and the non-dimensional shear stresses $\tau_{xy}^0 bh/P$ are anti-symmetrical about the y-axis. The distribution of the non-dimensional normal stresses is mainly affected by the axial load. When a concentrated axial load is applied, the magnitude of the non-dimensional normal and shear stresses in the vicinity of the concentrated load is large, but is very small at the area farthest away from the load. No singularity of the stresses occurs. When a uniform axial load is applied, the non-dimensional normal stresses $\sigma_x^0 bh/P$ are anti-symmetrical about the x-axis, and their magnitude gradually decreases as the area is far away from the top or bottom side. The magnitude of the non-dimensional normal stresses $\sigma_y^0 bh/P$ gradually decreases as the area is far away from the top side. The magnitude of the non-dimensional shear stresses $\tau_{xy}^0 bh/P$ decreases as the area is far away from the lateral side. The magnitude of the non-dimensional normal stresses $\sigma_x^0 bh/P$ and $\sigma_y^0 bh/P$ is larger than that of the non-dimensional shear stresses $\tau_{xy}^0 bh/P$. The affection zones of the non-dimensional normal stresses increase as the axial load changes from a concentrated load to a uniform load.

The buckling mode shapes of the plate for the loading cases $c/a = 0$, 0.5, and 1.0 are calculated and depicted in Fig. 11(a)–(c). The buckling mode shapes are less affected by the loadings, although the pre-buckling stresses are much affected by them.

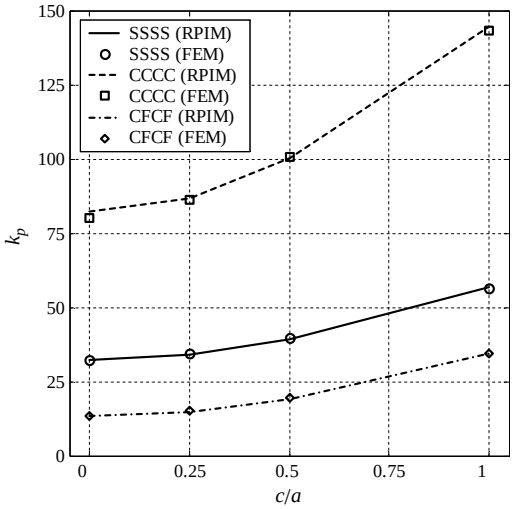

Fig. 12. The buckling load parameters of the square plate that is subjected to axial and shear in-plane edge loadings.

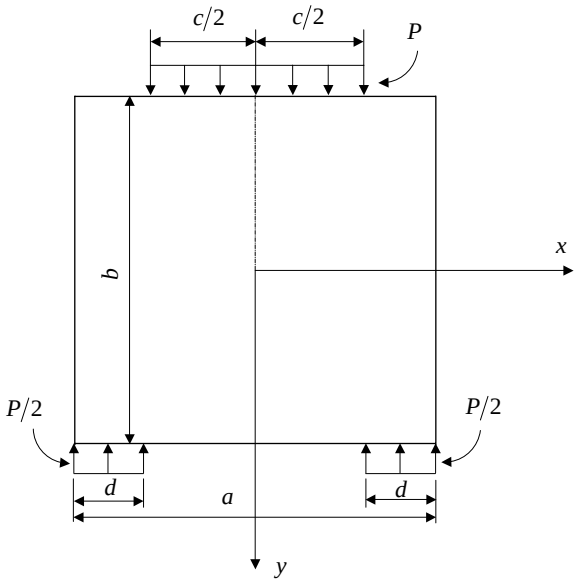

Fig. 13. A square plate that is subjected to two opposite in-plane edge loadings.

The buckling loads for the loading cases $c/a = 0$, 0.25, 0.5, and 1.0 are computed using the RPIM and *ANSYS*. The results are presented in Table 3 and Fig. 12, and the RPIM buckling load parameters are in excellent agreement with the FEM results. The buckling load parameters increase as the axial load changes from a concentrated load to a uniform load. The affection zones of the pre-buckling normal and shear stresses are very small for the concentrated axial load, but the buckling load parameter is also small. Therefore, increasing the distribution zone of pre-buckling stresses in the plate can increase the buckling load.

The third example is a square Mindlin plate, as shown in Fig. 13, that is subjected to two opposite in-plane edge loadings. The thickness ratio of the plate is $h/b = 0.01$. Three boundary conditions, SSSS, CCCC, and CFCF, are considered. Different in-plane edge loadings are applied to the plate through the changes of c/a and d/a. The buckling loads of the plate are calculated using the RPIM and *ANSYS*. The results are listed in Table 4 and shown in Fig. 14(a) and (b). The RPIM buckling load parameters agree very well with the FEM results.

Table 4
Buckling load parameters $k_p = P_{cr}b/D_0$ for a square Mindlin plate that is subjected to two opposite in-plane edge loadings ($h/b = 0.01$)

c/a	d/a	Boundaries		
		SSSS	CCCC	CFCF
0	0	28.650 (28.773[a])	72.237 (70.599[a])	13.656 (13.450[a])
	0.25	28.762 (29.227[a])	73.625 (71.936[a])	13.682 (13.459[a])
0.25	0	30.766 (30.485[a])	75.567 (75.105[a])	16.121 (15.925[a])
	0.25	31.027 (30.949[a])	77.203 (76.652[a])	16.262 (16.075[a])
0.5	0	34.047 (34.165[a])	84.647 (84.418[a])	20.799 (20.833[a])
	0.25	34.626 (34.810[a])	86.570 (86.363[a])	20.994 (21.066[a])
1.0	0	44.012 (44.359[a])	105.837 (105.600[a])	39.477 (39.675[a])
	0.25	44.861 (44.609[a])	107.821 (107.497[a])	39.829 (40.084[a])

[a] Results of FEM (*ANSYS*).

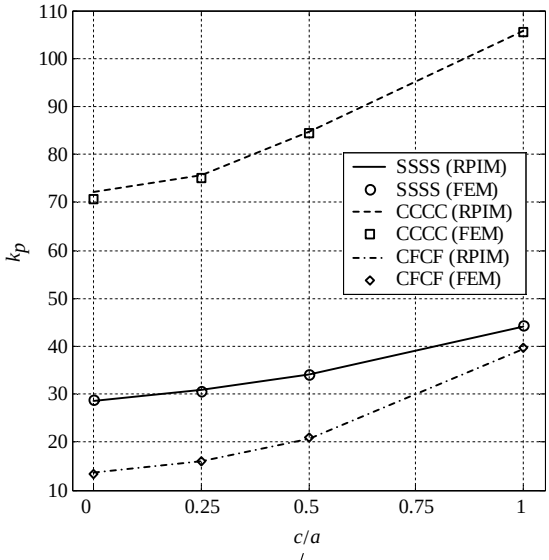

(a) $d/a = 0$

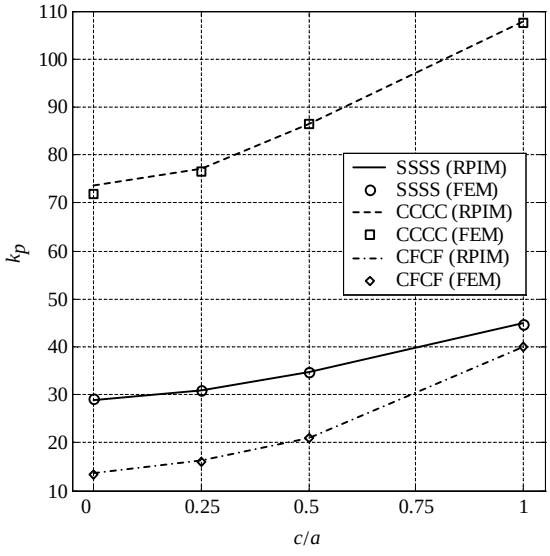

(b) $d/a = 0.25$

Fig. 14. The buckling load parameters of the square plate that is subjected to two opposite in-plane edge loadings.

5. Conclusions

The buckling loads of the Mindlin plates that are subjected to non-uniform in-plane edge loadings are computed by employing a newly developed RPIM. The displacement in the RPIM is interpolated according to a set of scattered nodes instead of elements. It makes the RPIM flexible. The RPIM can avoid the

disadvantages that arise in the FEM from the use of elements, e.g., remeshing in the FEM is often required to avoid heavily distorted elements and ensure the accuracy of results. The RPIM can easily control the location and number of nodes, e.g., one can easily add new nodes for buckling load calculation in the distribution of nodes for pre-buckling stress calculation. One can also easily adjust the nodal distribution for the desired computational accuracy, e.g., one can let the density of nodes near the concentrated load be higher without complex processes. The interpolated displacements can be easily approximated in a higher desired order by taking more nodes in the influence domain. The RPIM imposes essential boundary conditions similar to the FEM. The study shows that the RPIM with the MQ radial basis function offers good accuracy. For pre-buckling stress calculation, no stress singularity occurs when a concentrated load is applied. The RPIM uses fewer nodes to obtain the same level of accuracy as the FEM. Hence, the RPIM is efficient for solving the buckling loads of the Mindlin plates that are subjected to non-uniform in-plane edge loadings.

References

Belytschko, T., Lu, Y.Y., Gu, L., 1994. Element-free Galerkin methods. International Journal for Numerical Methods in Engineering 37, 229–256.

Cheung, Y.K., Zhou, D., 2002. Three-dimensional vibration analysis of cantilevered and completely free isosceles triangular plates. International Journal of Solids and Structures 39, 673–687.

Golberg, M.A., Chen, C.S., Bowman, H., 1999. Some recent results and proposals for the use of radial basis functions in the BEM. Engineering Analysis with Boundary Elements 23, 285–296.

Hardy, R.L., 1990. Theory and applications of the multiquadrics-biharmonic method (20 years of discovery 1968–1988). Computers and Mathematics with Applications 19, 163–208.

Kansa, E.J., 1990. Multiquadrics—a scattered data approximation scheme with applications to computational fluid dynamics, I: Surface approximations and partial derivative estimates. Computers and Mathematics with Applications 19 (8/9), 127–145.

Kitipornchai, S., Xiang, Y., Wang, C.M., Liew, K.M., 1993. Buckling of thick skew plates. International Journal for Numerical Methods in Engineering 36, 1299–1310.

Leissa, A.W., Ayoub, E.F., 1988. Vibration and buckling of a simply supported rectangular plate subjected to a pair of in-plane concentrated forces. Journal of Sound and Vibration 127 (1), 155–171.

Liew, K.M., Xiang, Y., Kitipornchai, S., 1995. Research on thick plate vibration: a literature survey. Journal of Sound and Vibration 180 (1), 163–176.

Liew, K.M., Xiang, Y., Kitipornchai, S., 1996. Analytical buckling solutions for Mindlin plates involving free edges. International Journal of Mechanical Sciences 38 (10), 1127–1138.

Liew, K.M., Huang, Y.Q., Reddy, J.N., 2002a. A hybrid moving least squares and differential quadrature (MLSDQ) mesh-free method. International Journal of Computational Engineering Science 2, 1–12.

Liew, K.M., Ng, T.Y., Wu, Y.C., 2002b. Meshless method for large deformation analysis—a reproducing kernel particle method. Engineering Structures 24, 543–551.

Liew, K.M., Ng, T.Y., Zhao, X., Reddy, J.N., 2002c. Harmonic reproducing kernel particle method for free vibration analysis of rotating cylindrical shells. Computer Methods in Applied Mechanics and Engineering 191, 4141–4157.

Liew, K.M., Wu, Y.C., Zou, G.P., Ng, T.Y., 2002d. Elasto-plasticity revisited: numerical analysis via reproducing kernel particle method and parametric quadratic programming. International Journal for Numerical Methods in Engineering 55, 669–683.

Liu, W.K., Jun, S., Zhang, Y.F., 1995. Reproducing kernel particle methods. International Journal for Numerical Methods in Fluids 20, 1081–1106.

Nayroles, B., Touzot, G., Villon, P., 1992. Generalizing the finite element method: diffuse approximation and diffuse elements. Computational Mechanics 10, 307–318.

Timoshenko, S.P., James, M.G., 1985. Theory of Elastic Stability. McGraw-Hill, Singapore.

Wang, J.G., Liu, G.R., 2002. A point interpolation meshless method based on radial basis functions. International Journal for Numerical Methods in Engineering 54, 1623–1648.

Wang, C.M., Liew, K.M., Xiang, Y., Kitipornchai, S., 1993. Buckling of rectangular Mindlin plates with internal line supports. International Journal of Solids and Structures 30 (1), 1–17.